

Chapter 2

The effect of specular reflection on spaceborne lidar measurements of ice clouds

Summary. Specular reflection from horizontally aligned crystals can cause an anomalously high backscatter when observed by lidar pointing precisely at zenith or nadir, but the effect can be essentially eliminated by changing the orientation of the lidar by a few degrees. As this enhanced return is not accompanied by any increase in extinction, it can make interpretation of the lidar echo in terms of cloud radiative properties problematic, so is of concern for spaceborne cloud lidar missions. After reviewing some of the existing work on lidar specular reflection, we compare distributions of integrated backscatter measured from 80 days of zenith-pointing 905-nm lidar observations at Chilbolton in Southern England to 60 days of data measured at 5° from zenith, from which the effect of specular reflection on the extinction-to-backscatter ratio can be estimated. The results indicate that specular reflection was present to some degree in over 50% of the ice profiles observed at zenith, and in 20% of the profiles the integrated backscatter associated with the phenomenon was considerably higher even than liquid water clouds, which normally tend to be much more reflective than ice. One percent of the profiles had an integrated backscatter greater than 0.2 sr^{-1} corresponding to a profile-mean extinction-to-backscatter ratio of less than 2.4 sr. A simple algorithm was used to estimate the height distribution of the regions of strongest specular reflection. It was found that specular reflection tends to be much stronger and more common at temperatures between -20°C and -5°C , with a maximum at -12°C . This is presumably because plate crystals, which give the greatest specular signal, tend to be found in this range. It is recommended that spaceborne lidars point at least 1° from nadir to avoid this phenomenon.

2.1 Introduction

Two spaceborne lidar missions are currently in the planning stage which have among their primary aims the global measurement of ice clouds. The NASA *Calipso* lidar is due for launch in 2005 and will be complemented by the radar on board *CloudSat*, while ESA and NASDA are considering the *EarthCARE* mission which would involve a lidar and radar on the same platform. In January 2003 the *IceSat* lidar was launched, which has as one of its secondary mission goals the quantitative measurement of ice clouds. All these lidars are currently planned to be nadir pointing. It has been known for at least 25 years that specular reflection from horizontally aligned crystals can cause an enhanced return for lidars pointing exactly at zenith or nadir (Sassen 1977, Platt 1977, Gibson et al. 1977), so it is important to determine

whether problems associated with this phenomenon are severe enough that they would compromise the ability of the lidar to infer the important properties of the cloud, particularly those relating to radiative transfer.

We first consider the angular dependence of specular reflection. It is well known that ice crystals often tend to fall with their longest axis horizontal. Platt et al. (1978) compared lidar observations of a particular ice cloud at 0° , 0.5° , 2° and 8° from zenith and found that the backscattered intensity fell to 3% of its zenith value at 0.5° from vertical. Similarly, Thomas et al. (1990) reported that the backscattered intensity at certain heights in an ice cloud fell to 5% of the zenith value when they offset their lidar by 0.3° . Hence if the distribution of crystal canting angles were to be modelled by a Gaussian, we would infer a standard deviation of 0.12° – 0.19° . It should be noted that other optical methods have tended to find higher ice-crystal canting angles. For example, McDowell (1979) reported angles of around 1° from observations of the circumzenithal arc, Chepfer et al. (1999) used POLDER satellite data at various angles of incidence to suggest a maximum value of 2.5° , while Sassen (1980) deduced a maximum of 3° from analysis of ‘light pillars’ from specular reflection of sunlight. Nonetheless, it would seem best to use the results of direct observations of specular reflection to decide what pointing angle is necessary in order to avoid it.

Thomas et al. (1990) reported that specular reflection occurred to some degree in 50% of lidar profiles in ice cloud, and that it could occur at any temperature between -5°C and -70°C . Their dataset consisted of observations from all seasons. In this study we use the integrated backscatter to show how strong specular reflection can be identified in zenith-pointing lidar data without the need to compare zenith and off-zenith observations of the same cloud. After describing the algorithm in section 2.2, we compare the statistics obtained from continuous periods of zenith and off-zenith observation. Then in section 2.4 we discuss the implication of these results for spaceborne lidar measurements.

2.2 Method

We now describe the algorithm used to judge which clouds are composed of specularly reflecting crystals. Lidar measures attenuated backscatter coefficient, β' , which is related to true backscatter coefficient, β , by

$$\beta'(z) = \beta(z)e^{-2\eta\tau(z)}, \quad (2.1)$$

where $\tau(z)$ is the optical depth of the atmosphere at 905 nm between the lidar and the point of observation at height z . We follow Platt (1973) and represent multiple scattering by the single factor η , which can take a value between 0.5 and 1 depending on the specifications of the lidar and the nature of the cloud particles. For the specifications of the Vaisala CT75K lidar used in this study, calculations using the model of Eloranta (1998) indicate that the factor η is approximately constant at 0.7 ± 0.04 for measurements at a range greater than 2 km (Hogan et al. 2003)

Platt (1973) was the first to demonstrate that the integral of the β' through a completely attenuating cloud is equal to $(2\eta k)^{-1}$, where k is the extinction-to-backscatter ratio (or ‘lidar ratio’) of the cloud particles. Calculations using Mie theory indicate that for distributions of liquid water droplets with median volumetric diameter in the range 5–50 μm , k at 905 nm is approximately constant at 18.75 sr. Therefore the integrated backscatter measured by the Chilbolton lidar through optically thick liquid clouds such as stratocumulus tends to be close to 0.038 sr^{-1} . This property is used to calibrate the instrument (O’Connor et al. 2003).

For ice particles not observed from zenith or nadir, k spans perhaps a factor of two, but specularly reflecting crystals are characterized by an enhanced backscatter with no associated increase in extinction,

i.e. an anomalously low value of k . Therefore, a tell-tale sign of specular reflection is that the integrated backscatter significantly exceeds the value for liquid water droplets. Integrated backscatter observations by the Chilbolton lidar pointing at 5° from zenith indicate that the k of ice usually lies between 10 and 20 sr.

Because we are interested in determining the fraction of clouds that contain specularly reflecting crystals, we restrict our analysis to clouds above 2 km; below this height the lidar also detects boundary layer aerosol which can sometimes be difficult to distinguish from cloud. The melting layer was below 2 km throughout the period of the analysis. Each profile of β' is integrated from 2 km up to the highest range gate, and profiles for which the integral is more than 0.042 sr^{-1} (10% more than the theoretical value for fully attenuating liquid water cloud) are deemed to contain specular reflection at some altitude. It is then assumed that the pixels with the highest values of β' in the profile are responsible for all the specular reflection, so the β' values are selected in order, starting with the largest, and summed until the excess above this 0.042 sr^{-1} value is accounted for. These selected pixels are flagged as containing specularly reflecting crystals. However, it is not uncommon for a mid-level cloud to be topped by a layer of supercooled liquid water 100–200 m thick with high backscatter coefficient. We therefore make the following simple modification to the technique so that liquid water layers at cloud top are not selected, and specular reflection is attributed correctly to purely ice regions. The integrated backscatter through the highest 200 m of detected cloud is calculated and if it exceeds 40% of the 0.038 sr^{-1} expected for liquid water then it is removed from consideration. The 40% factor allows for some attenuation by the intervening ice cloud, while still providing a high threshold that purely ice at cloud top would not exceed.

It should be noted that this procedure may tend to underestimate the fraction of clouds containing specular reflection for two main reasons. Firstly, we are implicitly assuming the cloud to have a high optical depth so that the integrated backscatter can easily be interpreted in terms of k . In the case of clouds with a lower optical depth, specular reflection may be occurring but would be less likely to exceed the threshold value. Secondly, by attributing the specular reflection entirely to the pixels with the largest values of β' , we are neglecting the possibility that specular reflection is more evenly distributed through the profile, but at a lower intensity. Therefore the algorithm is just locating regions of “strong” specular reflection.

Two examples of the algorithm in operation are now shown. Figure 2.1a shows a 6-h time-height section of β' through altocumulus on 17 October 2002. The thin layer of high backscatter at cloud top is attributable to liquid water (Hogan et al. 2003), and in the first half of the period the integrated backscatter (Fig. 2.1b) is close to the theoretical value for liquid water of 0.038 sr^{-1} . In the second half of the period, the integral is dominated by the contribution from the ice particles falling beneath the liquid water, where it peaks at 8 times the liquid water value. Figure 2.1c shows in black where the algorithm has diagnosed the presence of specularly reflecting crystals; note that the high return at cloud top, believed to be due to liquid water, has been excluded. Figure 2.2 shows lidar observations of specular reflection in ice cloud associated with an approaching front, where the integrated backscatter reaches 6 times the value for liquid water. An interesting feature of this case at around 02:15 UTC is the presence of thin layers a few hundred metres thick, where the specular reflection apparently disappears for around 15 mins. It would seem very unlikely that the falling ice crystals change from plates to some other form and back to plates over such a short distance. A more likely explanation is that shear layers are present at these altitudes, which generate turbulence that perturb the crystals from horizontal alignment as they fall through it.

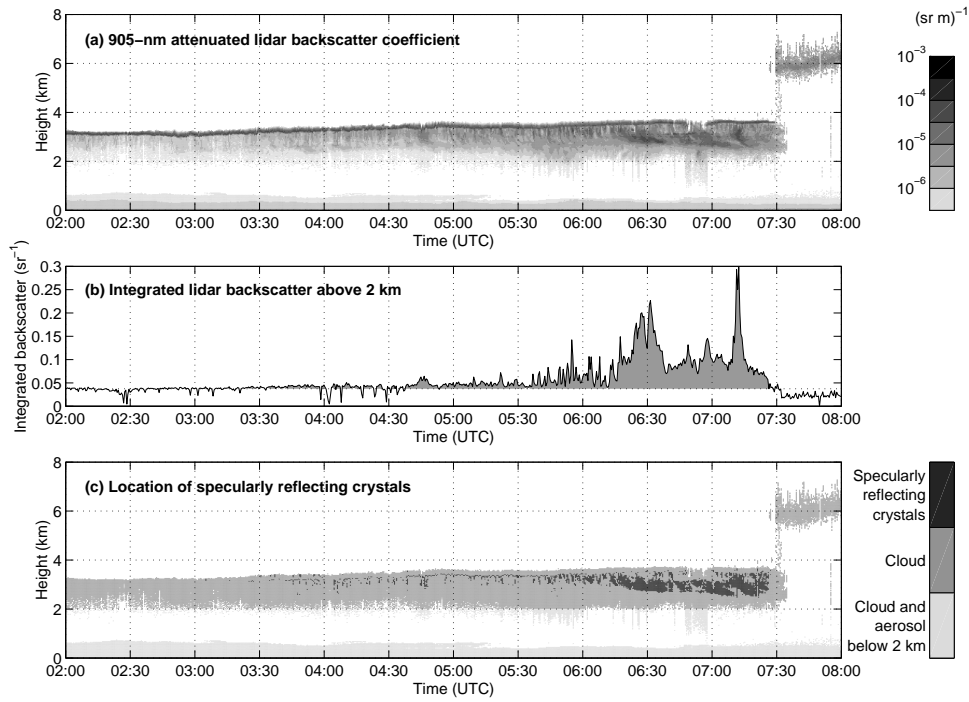


Figure 2.1: (a) Six-hour time-height section of β' measured at zenith by the Chilbolton lidar on 17 October 2002; (b) the integrated backscatter through the returns above 2 km, where the horizontal dotted line indicates the theoretical asymptote for completely attenuating liquid water cloud; (c) location of the regions of strong specular reflection.

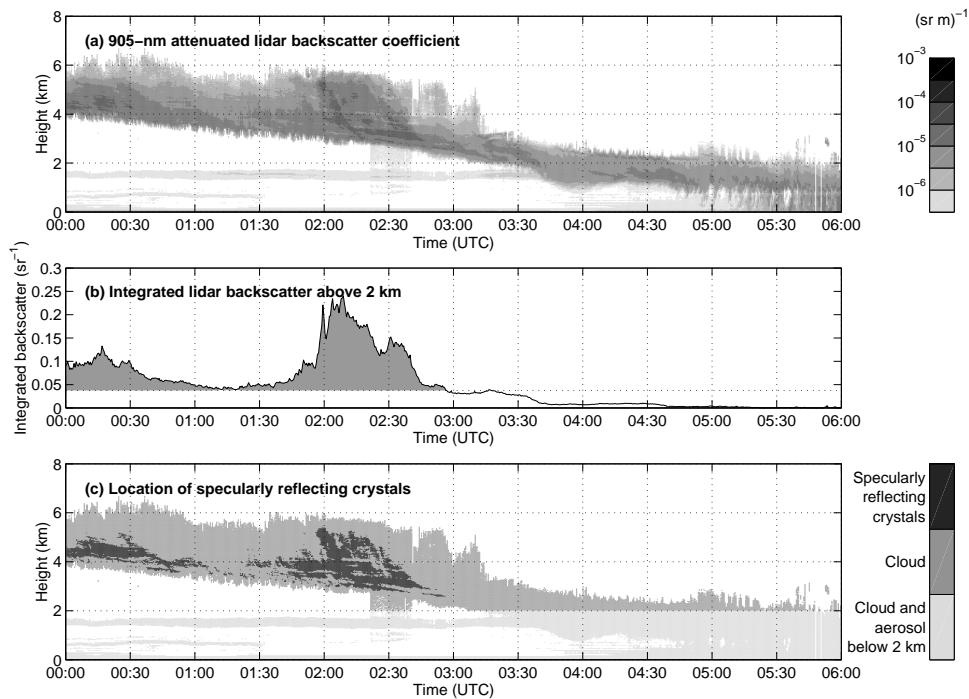


Figure 2.2: As Fig. 2.1, but for 20 October 2002.

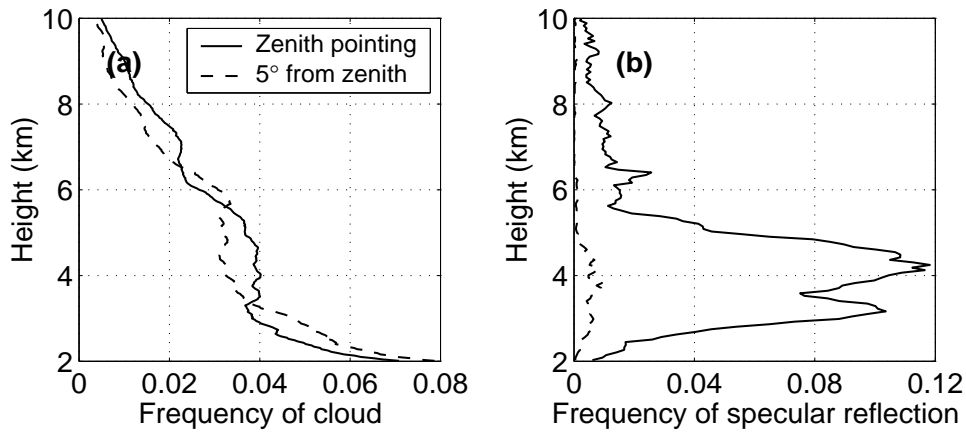


Figure 2.3: (a) Frequency that cloud was observed versus height for the zenith and off-zenith datasets; (b) frequency of strong specular reflection in the these clouds.

2.3 Results

We now summarize the findings from 80 days of data taken between 15 October 2002 and 14 April 2003 when the Chilbolton lidar was pointing directly at zenith. Every 30 s the instrument makes an internal measurement of elevation to 1° , and profiles not reported to be at zenith to within this precision were rejected. The resulting data are equivalent to 28 days of continuous observation. These are compared with 60 days of data from the autumns of 2000 and 2001, when the lidar was operating at 5° from zenith. Smaller subsets the observations show very much the same behaviour as the full dataset, indicating that the amount of data is sufficient to get a representative sample and therefore to compare statistics from two different periods.

Figure 2.3 depicts the frequency that cloud was observed and the fraction of those clouds that contained specular reflection, as a function of height. Cloud was deemed to be observed whenever β' was $7.5 \times 10^{-7} \text{ sr}^{-1} \text{ m}^{-1}$ or greater. Due to the frequent obscuration by low-level clouds, cloud was observed less than 10% of the time at any given height above 2 km, although there is no significant difference between the frequencies for zenith and off-zenith pointing.

Figure 2.3b shows a striking difference between the zenith and off-zenith results for the frequency of specular reflection; nearly 20% of clouds at 4 km observed at zenith triggered the algorithm, compared with 1% in the off-zenith data. The occurrence of specular reflection appears to be mostly confined between 2.5 and 5.5 km. Temperature profiles over Chilbolton from a forecast model (either the Met Office or European Centre for Medium Range Weather Forecasts (ECMWF) model, depending on availability) were used to bin the data by temperature, as shown in Fig. 2.4. It can be seen that the enhanced specular reflection is concentrated at temperatures warmer than -20°C , which can be explained by the fact that plate crystals, believed to be responsible for the strongest specular reflection, grow only in the temperature range -23°C to -9°C . The enhancement at temperatures warmer than -9°C is presumably due to sedimentation from above. The peak occurrence of specular reflection is at -12°C , which agrees with the finding of Sauvageot et al. (1986) from polarimetric radar that non-spherical horizontally aligned crystals occur more frequently at -12°C than at any other temperature.

We next consider the frequency distribution of integrated backscatter for cloudy profiles. As before, we consider only data above 2 km, and specify that a profile is cloudy if the optical depth exceeds 0.1; for $k = 18.75 \text{ sr}$, this corresponds to a threshold integrated backscatter of 0.005 sr^{-1} . Figure 2.5a depicts the cumulative probability of integrated backscatter values for the zenith and off-zenith datasets.

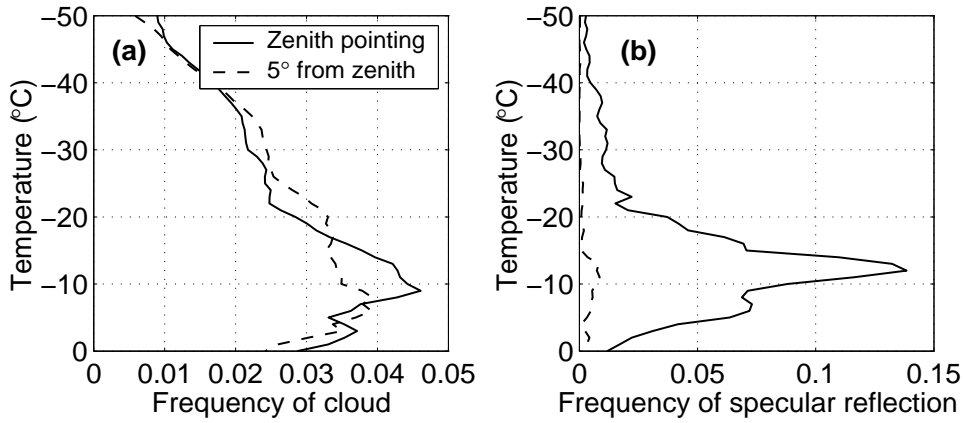


Figure 2.4: (a) Frequency that cloud was observed versus temperature for the zenith and off-zenith datasets; (b) frequency of strong specular reflection in the these clouds.

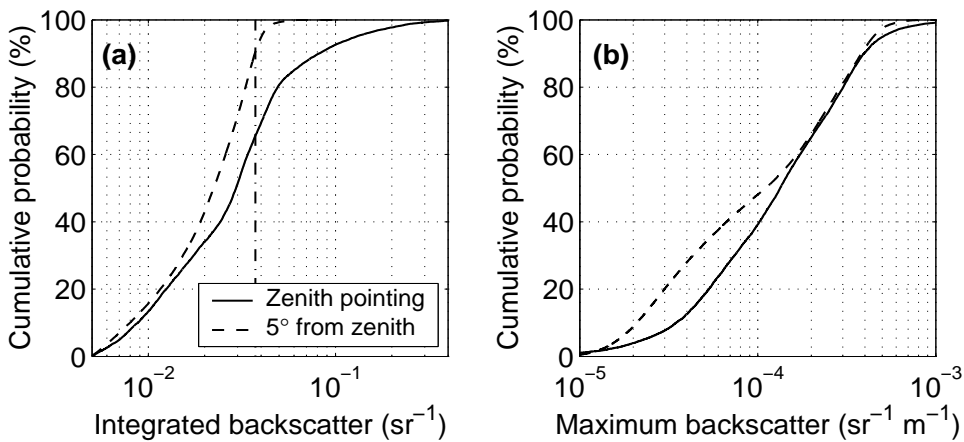


Figure 2.5: Cumulative probability statistics for cloudy profiles above 2 km, where a profile is declared cloudy if the integrated backscatter exceeds 0.005 sr^{-1} , equivalent to an optical depth of around 0.1: (a) integrated backscatter and (b) maximum backscatter in the profile.

The vertical dot-dashed line indicates the asymptote for optically thick liquid water cloud. As expected, the off-zenith observations are almost always smaller than this asymptote. It can be seen that the two lines sharply diverge in the highest quintile, where the integrated backscatter exceeds the value corresponding to liquid water clouds, thus indicating that specular reflection is strong in around 20% of profiles. However, the lines actually begin to diverge much sooner, suggesting that specular reflection is present at lower intensities in more than half of the cloudy profiles. This agrees with the findings of Thomas et al. (1990). It is notable that in around 1% of the profiles the integrated backscatter exceeds 0.3 sr^{-1} , corresponding to a k of as little as 2.4 sr. Ansmann et al. (1992) compared independent measurements of backscatter and extinction in cirrus, obtained from a zenith-pointing 308-nm Raman lidar. They found typical k values between 5 and 15 sr, but on one occasion strong specular reflection caused values as low as 2 sr at the top of a cirrus cloud.

Figure 2.5b shows the cumulative probability of the maximum value of β' in the profile. The distribution of values above $2 \times 10^{-4} \text{ s}^{-1} \text{ m}^{-1}$ is very much the same regardless of pointing angle, presumably because the very high backscatter coefficients nearly always correspond to liquid water clouds, the occurrence of which is the same in the two datasets. Specular reflection exhibits itself mostly as an

enhancement of the lower backscatter values, those between 2×10^{-5} and $2 \times 10^{-4} \text{ s}^{-1} \text{ m}^{-1}$, although there is also evidence for enhancement in the highest 5% of the data.

2.4 Discussion

We have shown that specular reflection can be a problem for interpreting lidar observations taken precisely at zenith or nadir. The algorithm presented here only detects strong specular reflection, but still demonstrates the problem very clearly. In summary, 20% of ice cloud profiles contain specular reflection strong enough that it could be detected in spaceborne lidar data using integrated backscatter (although not easily corrected), but at least 50% of profiles appear to exhibit specular reflection at a lower intensity, such that it would go undetected and could bias the retrievals. Low values of depolarization ratio can assist in identifying regions of specular reflection, but they are often difficult to distinguish from liquid water cloud.

The results of Platt et al. (1978) and Thomas et al. (1990) indicate that moving as little as 1° from zenith should be sufficient to reduce the effect to a level such that it does not introduce errors in k greater than the natural variability of k present in ice clouds. However, there are other constraints that must be brought into consideration, not least the need for co-location with other instruments. For instance, the proposed ESA *EarthCARE* satellite would carry a Doppler radar as well as a lidar on the same platform, and the radar has to look directly to nadir in order that the vertical velocity measurements are not contaminated by the horizontal wind and the motion of the spacecraft. Offsetting the lidar would complicate the processing system slightly as data would have to be shifted in time in order that synergetic algorithms can be applied, but for a 1° pointing angle from an orbit altitude of 400 km, this is only around a 1-s offset.

We now consider how spaceborne lidar data in ice cloud are to be used and what impact the anomalously low values of k would have. The principal problem to overcome in the analysis of lidar data is the attenuation of the lidar signal, and a major advance was made in the development of synergetic radar/lidar retrieval algorithms (e.g. Donovan and van Lammeren 2000, Tinel et al. 2000) that essentially use the radar to ensure that the lidar inversion is stable and that an accurate extinction profile is obtained. Studies have shown that these algorithms are insensitive to either the calibration of the lidar or to the absolute value of k , but that variations in k within a single profile will cause errors in the retrieved extinction profile. Therefore the most common error is likely to occur when a profile consists of two layers, one containing specularly reflecting crystals and the other containing none. In such a scenario the extinction of the former would be overestimated and that of the latter underestimated, with the biases in proportion to the error in k . This could bias both the longwave and shortwave fluxes, and hence the inferred heating profile. The dependence of specular reflection with height (Fig. 2.3) suggests that this would not be an uncommon scenario.

Figure 2.3 actually implies that at temperatures colder than -23°C , specular reflection is not a significant problem. This is at odds with previous studies and highlights the limitation of our algorithm in that it tends to detect specular reflection only in the more optically thick clouds. The statistics of these high clouds are also poor in our short dataset. Operation of two lidars side-by-side for a few months would be necessary to quantify the effect exactly.

References

Ansmann, A., U. Wandinger, M. Riebesell, C. Weitkamp and W. Michaelis, 1992: Independent measurement of extinction and backscatter profiles in cirrus clouds by using a combined Raman elastic-backscatter lidar. *Appl. Optics*, **33**, 7113–7131.

- Chepfer, et al., 1999: Observations of horizontally oriented ice crystals in cirrus clouds with POLDER-1/ADEOS-1. *J. Quant. Spectrosc.*, **63**, 521–543.
- Donovan, D. P., and A. C. A. P. van Lammeren, 2000: Combined lidar and radar cloud particle effective size retrievals made during CLARA. *Phys. Chem. Earth*, **25**, 115–120.
- Eloranta, E. W., 1998: A practical model for the calculation of multiply scattered lidar returns. *Appl. Optics*, **37**, 2464–2472.
- Gibson, A. J., L. Thomas and S. K. Bhattacharyya, 1977: Some characteristics of cirrus clouds deduced from laser radar observations at different elevation angles. *J. Atmos. Terr. Phys.*, **29**, 657–660.
- Hogan, R. J., A. J. Illingworth, E. J. O'Connor and J. P. V. Poiares Baptista, 2003: Characteristics of mixed-phase clouds - 2. A climatology from ground-based lidar. *Quart. J. Roy. Meteorol. Soc.*, **129**, 2117–2134.
- McDowell, R. S., 1979: Frequency analysis of the circumzenithal arc: evidence for the oscillation of ice crystal plates in the upper atmosphere. *J. Opt. Soc. Am.*, **69**, 1119–1122.
- O'Connor, E. J., A. J. Illingworth and R. J. Hogan, 2003: A technique for auto-calibration of cloud lidar. *Submitted to J. Atmos. Oceanic Technol.*
- Platt, C. M. R., 1973: Lidar and radiometric observations of cirrus clouds. *J. Atmos. Sci.*, **30**, 1191–1204.
- Platt, C. M. R., 1977: Lidar observation of a mixed-phase altostratus cloud. *J. Appl. Meteorol.*, **16**, 339–345.
- Platt, C. M. R., N. Abshire and G. McNice, 1978: Some microphysical properties of an ice cloud from lidar observation of horizontally aligned crystals. *J. Appl. Meteorol.*, **17**, 1220–1224.
- Sassen, K., 1977: Ice crystal habit discrimination with the optical backscatter depolarization technique. *J. Appl. Meteorol.*, **16**, 425–431.
- Sassen, K., 1980: Remote sensing of planar ice crystal fall attitudes. *J. Meteorol. Soc. Japan*, **58**, 422–429.
- Sauvageot, H., K. Kouadio and C. Etty, 1986: The influence of temperature and supersaturation on the polarization of radar signals. *Proc. 23rd AMS Conf. on Radar Meteorol.*, Snowmass, CO, 173–176.
- Thomas, L., J. C. Cartwright and D. P. Wareing, 1990: Lidar observations of the horizontal orientation of ice crystals in cirrus clouds. *Tellus*, **42B**, 211–216.
- Tinel, C., J. Testud, A. Guyot and K. Caillault, 2000: Cloud parameter retrieval for combined remote sensing observations. *Phys. Chem. Earth*, **25**, 1063-1067.